



Bioinspired zero-energy thermal-management device based on visible and infrared thermochromism for all-season energy saving

Quan Zhang^{a,1}, Yufeng Wang^{a,1}, Yiwen Lv^a, Shixiong Yu^a, and Rujun Ma^{a,2}

Edited by David Weitz, Harvard University, Cambridge, MA; received April 28, 2022; accepted August 14, 2022

Radiative thermal management provides a zero-energy strategy to reduce the demands of fossil energy for active thermal management. However, whether solar heating or radiative cooling, one-way temperature control will exacerbate all-season energy consumption during hot summers or cold winters. Inspired by the Himalayan rabbit's hair and *Mimosa pudica*'s leaves, we proposed a dual-mode thermal-management device with two differently selective electromagnetic spectrums. The combination of visible and infrared "thermochromism" enables this device to freely switch between solar heating and radiative cooling modes by spontaneously perceiving the temperature without any external energy consumption. Numerical prediction shows that a dual-mode device exhibits an outstanding potential for all-season energy saving in terms of thermal management beyond most static or single-wavelength, range-regulable, temperature-responsive designs. Such a scalable and cost-efficient device represents a more efficient radiative thermal-management strategy toward applying in a practical scenario with dynamic daily and seasonal variations.

solar heating | radiative cooling | thermochromism | zero-energy consumption | shape memory polymer

Thermal management, including heating and cooling, plays an important role in human productive activities and daily life (1, 2). To meet diverse requirements in different situations, various thermal-management strategies have been designed and widely applied in practice (3–7). According to statistics, the total energy demand in 2019 is close to a 15-billion-ton oil equivalent (8), and approximately half of global final energy consumption is used for heating and cooling (9). It is a substantial figure and predicted to keep growing in the short term. Meanwhile, most of the energy for thermal management comes from either fossil fuels or inefficient uses of biomass, often accompanied by a large amount of carbon dioxide emission. This accounts for over 40% of global energy-related carbon dioxide emissions and has a potentially harmful effect on climate change (9). Therefore, it is important and imperative to develop low-energy or even zero-energy thermal-management technologies with renewable and clean energy.

A remarkable global average heating power on the earth supplied by inexhaustible solar radiation is 340 W/m² in the manner of solar-thermal conversion, and the extremely cold outer space could absorb enormous outgoing thermal radiation from the earth (10). If this heat source (the sun, ~5,800 K) and cold reservoir (outer space, ~3 K) in nature are fully utilized, they will effectively reduce the energy demands for thermal management (11). Radiative thermal management, a combined strategy of solar heating and radiative cooling, has emerged and gained more prominence recently. Differing from active thermal management, radiative thermal management, as a kind of passive thermal management, could complete the heat-transfer process by relying solely on the thermal dynamics of radiation without any external energy consumption. To realize this goal, two sets of opposite, highly selective electromagnetic spectrums are essential (12–15). For ideal solar heating, the materials should have high solar absorption (0.4–2.5 μm) and low infrared emission (2.5–15 μm) (16). For ideal radiative cooling, the materials should reflect solar radiation as much as possible and strongly release heat by infrared radiation (17). However, an unavoidable challenge is that the environment and climate in the real world are dynamic (18). This requires that a zero-energy thermal-management device not only have the above two sets of electromagnetic spectrums, but also be able to automatically switch them by spontaneously perceiving the change in the environment.

Various stimulus-responsive (including temperature (19–31), humidity (32, 33), light (34), and other stimuli (35–37)) devices have been developed, which spontaneously modulate their spectral characteristics to realize passive thermal management, but without any external energy consumption. Compared with devices responding to other stimuli, the

Significance

The conflict between the static spectral characteristics of single-mode radiative thermal-management materials and the dynamic ambient temperature in the real world is an unavoidable problem in the future application of radiative thermal-management technology. Inspired by various biological stress responses in nature, we demonstrate a zero-energy, dual-mode, radiative, thermal-management device based on visible and infrared "thermochromism," which can switch to the right mode by spontaneously perceiving temperature change. For infrared thermochromism, in particular, the modulation of infrared emissivity is achieved by morphological evolution, like the opening-folding movement of *Mimosa pudica*'s leaves. This design provides a unique strategy for dynamic dual-mode radiative thermal management with zero energy consumption and shows a great potential for all-season energy saving.

Author contributions: Q.Z. and R.M. designed research; Q.Z., Y.W., Y.L., and S.Y. performed research; Q.Z., Y.W., Y.L., and S.Y. contributed new reagents/analytic tools; Q.Z., Y.W., Y.L., S.Y., and R.M. analyzed data; and Q.Z., Y.W., Y.L., S.Y., and R.M. wrote the paper.

The authors declare no competing interest.

This article is a PNAS Direct Submission.

Copyright © 2022 the Author(s). Published by PNAS. This article is distributed under [Creative Commons Attribution-NonCommercial-NoDerivatives License 4.0 \(CC BY-NC-ND\)](https://creativecommons.org/licenses/by-nc-nd/4.0/).

¹Q.Z. and Y.W. contributed equally to this work.

²To whom correspondence may be addressed. Email: malab@nankai.edu.cn.

This article contains supporting information online at <http://www.pnas.org/lookup/suppl/doi:10.1073/pnas.2207353119/-DCSupplemental>.

Published September 12, 2022.

temperature-responsive device is a more promising strategy to continuously control temperature, because the ultimate goal of thermal management is temperature control. The fluctuation of temperature may not ensure the changes in other stimuli, such as humidity or light, because there is no necessary connection between them. Currently, temperature-responsive thermal-management devices can be roughly divided into three categories according to modulating type of spectral characteristics: thermochromic window (high and low solar transmission) (19–25), thermochromic coating (high and low solar absorption) (26), and infrared modulator (high and low infrared radiation) (27–30) (Table 1). By comparison, current designs modulate spectral characteristics only for an individual wavelength range, rather than its entire electromagnetic spectrum from visible to infrared simultaneously. It means that these designs are only able to change the power of heating or cooling in one way, but cannot realize a real sense of switch between heating and cooling modes by perceiving temperature. Undesirable solar heating (radiative cooling) will exacerbate energy consumption for cooling (heating) and offsets the heating (cooling) energy saved in cold winter (hot summer). Therefore, more high-performance temperature control results will be realized by making full use of the sun and outer space if the thermal-management device has the ability to individually and simultaneously modulate its spectral characteristics in the wavelength range of solar and infrared radiation.

Herein, to address the aforementioned issue, we proposed a dynamic dual-mode thermal-management device. The spectral characteristics in solar and infrared regions are modulated separately, inspired by the color change of the Himalayan rabbit's hair and folding-opening movement of *Mimosa pudica's* (*M. pudica's*) leaves, respectively. The device could spontaneously switch from the heating mode of high solar absorption and low infrared emission to the cooling mode of high solar reflection and high-infrared emission without any external energy consumption when temperature increases and vice versa. Numerical prediction indicates that our device has the greatest potential of all-season energy saving in temperature control, compared with the temperature-responsive thermal-management devices reported in the literature.

Results

Bioinspired Design of Visible and Infrared “Thermochromism.”

The fascinating dynamic self-adaptive behavior of natural living things represents a creative source of inspiration for intelligent thermal-management strategies (38–41). For example, the color of the Himalayan rabbit's hair is temperature sensitive. When the weather is warm, the color of the hair is always white, and when it is cold, the hair on some tissues, including the nose,

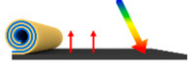
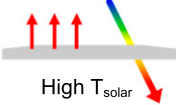
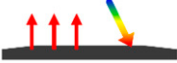
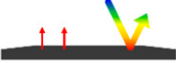

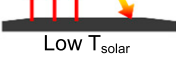


ears, feet, and tail, is dark. The different hair color maintains the temperature of these structures, fluctuating in a comfortable zone by modulating solar-thermal conversion efficiency. Another example is *M. pudica's* leaves, whose folding behavior could be triggered by various stimuli, such as touching, warming, blowing, and shaking. The photosynthesis rate of folded leaves is obviously lower than that of the open leaves (42). Besides reducing the damage of leaves, an additional result from the folding-opening movement of *M. pudica's* leaves realizes the functional regulation, that is, the modulation of the rate of photosynthesis. Combined with the color change of the Himalayan rabbit's hair and the folding-opening movement of *M. pudica's* leaves, visible thermochromism and infrared thermochromism are integrated into a dual-mode thermal-management strategy, which could take full advantage of solar radiation energy and extremely cold outer space by spontaneously adjusting the spectral characteristics (Fig. 1).

We proposed a dynamic dual-mode thermal-management device comprising a temperature-sensitive actuator with high-infrared emissivity and a same-sized visible thermochromic substrate with low-infrared emissivity (Fig. 1*A* and [Movie S1](#)). In this design, visible thermochromic substrate has a temperature-dependent solar absorption, while thermochromic powders attached to the substrate are like the pigments in the hair of the Himalayan rabbit (Fig. 1*B*). The change of solar absorptivity determines the increasing amount of internal energy of the device from solar-thermal conversion. On the other hand, the actuator could adjust its area covering the substrate by responding to the change of temperature, reminiscent of the coiling-unfolding behavior of the *M. pudica's* leaves (Fig. 1*C*). For the goal of regulating infrared emission, the substrate is required to have an infrared emission as low as possible while the actuator has a near-perfect infrared emissivity. In this way, the area of the actuator covering the substrate essentially decides the amount of heat that is transferred out from the device in the form of thermal radiation. Generally, this design realizes thermochromism in a broader wavelength range from visible to infrared by combining two unique biologic behaviors (temperature-dependent color of the Himalayan rabbit's hair and folding-opening movement of *M. pudica's* leaves). This is expected to be a possible thermal-management strategy without any external energy consumption to get better temperature control effects.

Design of Bionic Actuators Inspired by *M. pudica's* Leaves.

Infrared thermochromism is realized by changing the area of low-emissivity material covered by high-emissivity material, which is reminiscent of the folding-opening behavior of

Table 1. Spectral characteristics comparison of the typical temperature-responsive dynamic thermal-management devices in this work and reported in the literature

	This work	Thermochromic window (22)	Thermochromic coating (26)	Infrared modulator (27)
Heating mode	 High α_{solar} and low $\epsilon_{\text{infrared}}$	 High T_{solar}	 High α_{solar}	 Low $\epsilon_{\text{infrared}}$
Cooling mode	 High R_{solar} and high $\epsilon_{\text{infrared}}$	 Low T_{solar}	 High R_{solar}	 High $\epsilon_{\text{infrared}}$

→ Solar radiation, → Infrared radiation.

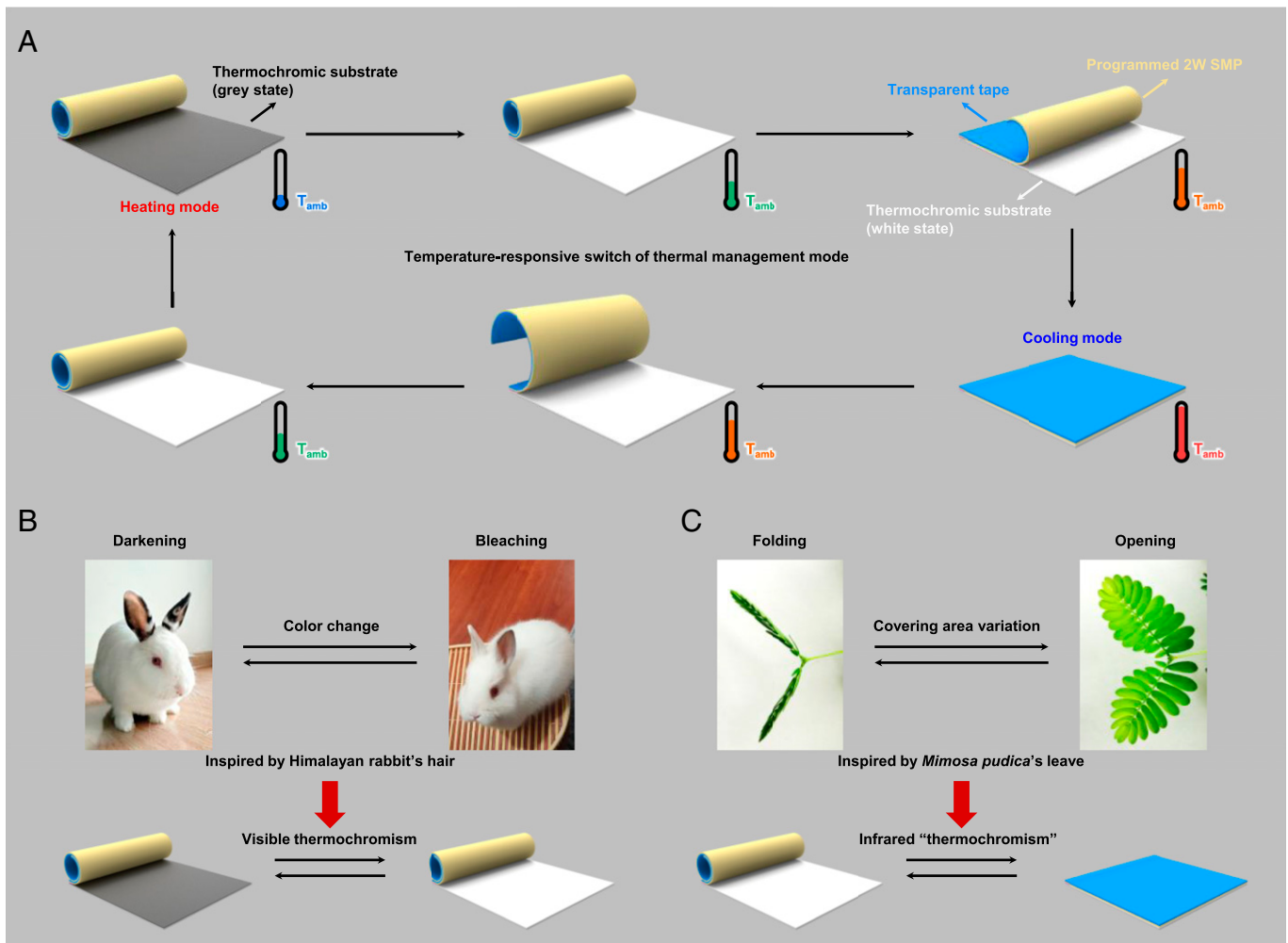


Fig. 1. Design principle of the dual-mode thermal-management device based on visible and infrared “thermochromism.” (A) The device consists of two main functional layers: a temperature-sensitive actuator with high-infrared emissivity composed of transparent tape and programmed 2W SMP and a thermochromic substrate with low-infrared emissivity. (B) Visible thermochromism in thermochromic substrate is like temperature-dependent color evolution of the Himalayan rabbit’s hair. (C) Infrared thermochromism is realized by a temperature-sensitive actuator high-infrared emissivity layer, which mimics the folding-opening behavior of *Mimosa pudica*’s leaves.

M. pudica’s leaves (Fig. 1C). The bionic actuator with high-infrared emissivity is composed of transparent tape and programmed two-way shape memory polymer (2W SMP). The coil-unfolding behavior of the bionic actuator is the result of its spontaneous shape adjustment to minimize the internal stress at the interface between the transparent tape and the programmed 2W SMP at different temperatures. It requires that programmed 2W SMP, as the key component of the bionic actuator, needs to have a reversible shape change with temperature. On the contrary, transparent tape has a temperature-independent and constant length at different temperatures. Thus, there is inevitable internal stress generating at the interface between the transparent tape and programmed 2W SMP when heated or cooled, which causes the bionic actuator to adjust its appearance to eliminate this stress.

The 2W SMP is synthesized by a one-step esterification reaction between three monomers, polytetrahydrofuran (PTHF), polycaprolactone (PCL) or polycaprolactone glycol (PCL-diol), and hexamethylene diisocyanate (HDI), on the catalyst dibutyltin dilaurate (DBTDL). The reversible shape memory performance of 2W SMP is achieved after a programming process. Taking polymer with monomer PCL ($M_n = 36,000$) as an example, an as-prepared 2W SMP strip is first stretched to five times the

initial length at 90°C ($T_{\text{programming}}$) and then cooled down to room temperature (T_{low}) by keeping the stretching state (Fig. 2A). When the stretched 2W SMP film is placed on a 55°C (T_{high}) heating plate, there is a certain shrinkage along the stretching direction. After the programming treatment, the 2W SMP strip exhibits an abnormal and reversible thermomechanical behavior, namely, shrinking when heated and extending when cooled. This thermomechanical behavior is determined by the force balance between different segments in the programmed 2W SMP during the repeated heating-cooling process (43). Two separate groups of “melting-crystallization” peaks are shown in the differential scanning calorimetry curve, which correspond to two chain segments (PTHF segments with lower temperature and PCL [or PCL-diol] segments with higher temperature) (SI Appendix, Fig. S1) (44). Stretching at 90°C enhances the orientation of the segments in 2W SMP. This enhancement is still maintained when cooled down to room temperature. Compared with as-prepared 2W SMP, there is an obvious improvement of the crystallinity after stretching (SI Appendix, Fig. S2). Meanwhile, the input of stretching energy is stored in the 2W SMP in the form of elastic potential energy. When the stretched 2W SMP is heated to 55°C , the partial segments with lower “melting” temperature gradually soften. During this process, a

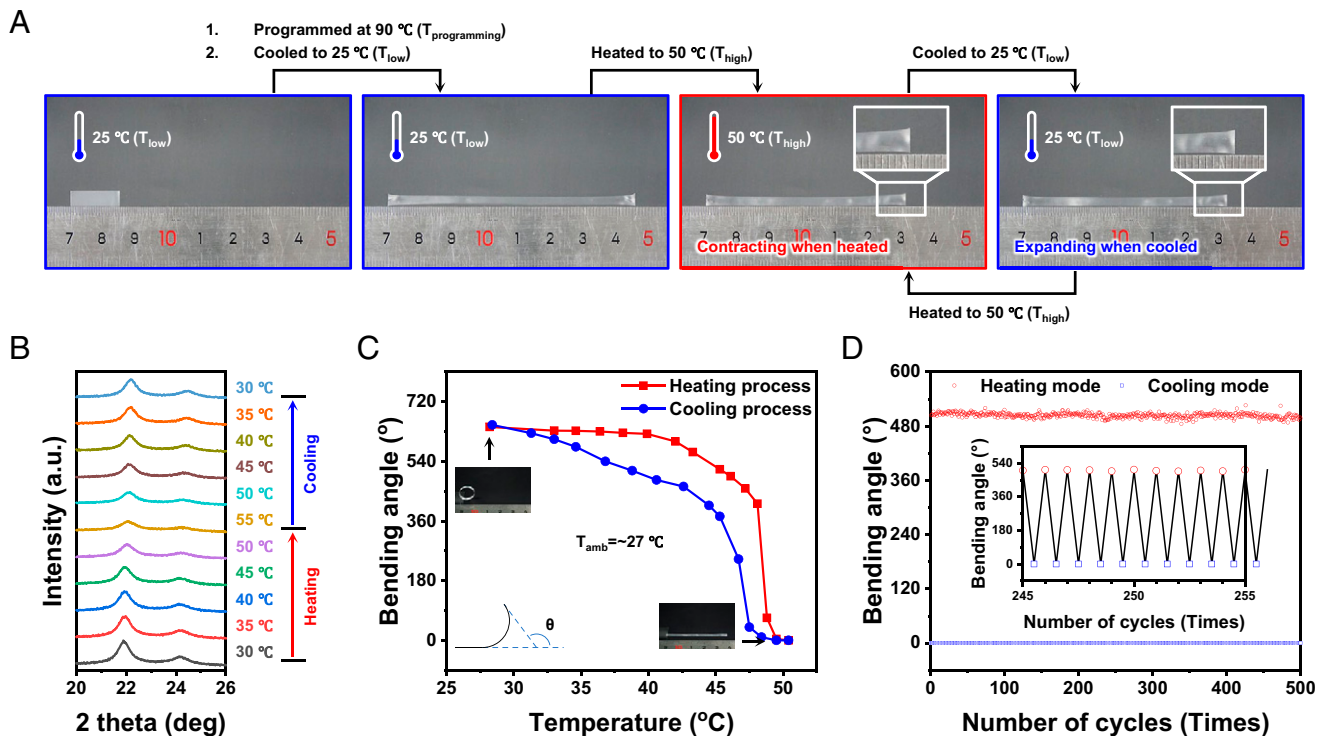


Fig. 2. Temperature-sensitive reversible shape memory performance. (A) Optical images showing the reversible shape memory effect of the 2W SMP strip after a programming process. (B) Temperature-dependent X-ray diffraction spectra of a programmed 2W SMP during a heating-cooling cycle. (C) The reversible bending performance of the transparent tape-2W SMP laminate at different temperatures. The molecular weight of PCL used for synthesis of 2W SMP is 36,000. (D) Long-term cyclability of transparent tape-2W SMP film between heating and cooling modes.

part of stored elastic potential energy in polymer molecular chains is released for force balance at the microscale, accompanying a certain degree of reduction of crystallinity (*SI Appendix*, Fig. S2). After the above programming treatment, the rest of elastic potential energy is stored in the 2W SMP for a long time, as long as the heating temperature is below the higher “melting” temperature. Fig. 2B shows a group of in situ X-ray diffraction (XRD) curves of the programmed 2W SMP during a complete heating-cooling process, which indicates that the crystallinity of PTHF segments depends on temperature (45). The crystallinity of PTHF segments gradually decreases with the increase of temperature. Conversely, it increases. This result means that the chain segments of PTHF will soften when heated, and the programmed 2W SMP will shrink to balance the rest of the elastic potential in the stretched molecules. When cooled, the programmed 2W SMP re-extends due to the recrystallization of PTHF chain segments.

After sticking a transparent tape on a same-sized programmed 2W SMP strip in the state of contraction, the transparent tape-2W SMP laminate exhibits a reversible coiling-unfolding morphology evolution. This is caused by the spontaneous minimization of the internal stress at the interface between transparent tape and programmed 2W SMP during reversible extension and shrinkage of programmed 2W SMP. The laminate could bend to the transparent tape side when cooled and fully flatten when heated, like the folding-opening behavior of the *M. pudica*'s leaves (*Movie S2*). As shown in Fig. 2C, the bending angle of the laminate is sensitive to temperature. With the temperature increase of the heating plate but lower than 39.9 °C, the bending angle is almost unchanged. Once the temperature is larger than 39.9 °C, especially above 48.1 °C, the bending angle decreases rapidly until the laminate fully unfolds. Furthermore, when the temperature decreases, the bending angle

continues to increase, corresponding to the laminate returning to its initial coiling state at room temperature again. During a heating-cooling process, a certain degree of hysteresis in the bending angle is related to the difference between the melting temperature and the crystallization temperature. For the 2W SMPs with the same molecular ratio among three monomers, both the crystallization temperature and melting temperature of two segments are increased with the molecular weight of PCL (or PCL-diol) monomer (*SI Appendix*, Fig. S1). It makes the responding temperature of transparent tape-2W SMP laminate adjustable, which covers a wider temperature zone, including the general human comfort zone (~ 26 °C) (*SI Appendix*, Fig. S3). Several transparent tape-programmed 2W SMP laminates are placed side by side and bonded together to form a sizable film. The 500 cycling test demonstrates that the film has excellent robustness of reversible shape memory, as does the laminate (Fig. 2D and *SI Appendix*, Fig. S4).

Visible and Infrared Thermochromism. A complete dual-mode thermal-management device consists of a temperature-sensitive actuator with high-infrared emissivity and a visible thermochromic substrate (Fig. 1). The mixing powders, including thermochromic powder and rutile titanium dioxide nanoparticles, are uniformly dispersed on a thin nitrile-butadiene rubber (NBR)-coated aluminum foil (Al foil), which is used as the visible thermochromic substrate. Meanwhile, a same-sized transparent tape-2W SMP film is used to realize infrared thermochromism. A narrow strip of very high bond (VHB) tape, as the only joint, fixes the temperature-sensitive actuator on the visible thermochromic material. As shown in Fig. 3A, the device in heating mode absorbs $\sim 73\%$ solar radiation in the visible region and has a lower midinfrared emission ($\sim 28\%$). Furthermore, for the cooling mode, the

device can reflect $\sim 65\%$ visible sunlight and has an extremely high midinfrared emissivity ($\sim 95\%$). However, there is a $\sim 38\%$ reduction of absorptivity for visible sunlight and $\sim 67\%$ enhancement of midinfrared emission, when the state of the device changes from heating mode to cooling mode.

Simultaneously captured optical images and infrared images visually present the change in spectral characteristics of the dual-mode device as a function of temperature. Two typical materials, the smooth Al foil with high reflectivity from the visible to the infrared region and light control aluminum wrap (LCAW) with high absorptivity/emissivity from the visible to infrared region, were chosen as references (*SI Appendix, Fig. S6*). In order to show the enhancement of infrared radiation when the device switches from heating mode to cooling mode at room temperature ($\sim 26^\circ\text{C}$), we deliberately used 2W SMP synthesized by PCL with a molecular weight of 36,000 rather than 10,000 in the subsequent experiments. Fig. 3*B* shows a group of optical images and infrared images. All of them are captured when the temperature of the sample is stable and close to that of the heating plate. It means that a sample with a lower infrared emissivity exhibits a lower measured temperature in infrared image and one with a higher emissivity is higher when the set emissivity of infrared camera remains constant ($\epsilon = 1$ in this work). As

a low-infrared emissive material, the surface temperature of Al foil measured in the infrared images at different temperatures of the heating plate does not change significantly. On the contrary, LCAW in the infrared images shows a measured temperature close to that of the heating plate at different temperatures. Meanwhile, the colors of Al foil and LCAW in optical images are both unchanged at room temperature and heating state. For the thermochromic layer (TC layer), its color distinctly changes from gray to white and then maintains when the temperature of the heating plate increases from 30°C to 40°C . In addition, its measured surface temperature in the infrared images is always lower than that of LCAW. This indicates that the TC layer has a lower midinfrared emissivity compared with LCAW all the time, although its emissivity is slightly higher than that of Al foil. These results show that temperature mainly determines the absorption of visible sunlight by TC layer, while having almost no influence on its infrared emission (*Movie S3*).

On this basis, we further compared the morphology evolution of a complete dual-mode device described in the optical and infrared images when the heating plate was heated to different temperatures (Fig. 3*C*). When the temperature of the heating plate increased from 30°C to 35°C , only visible thermochromism appeared in the TC layer of the dual-mode

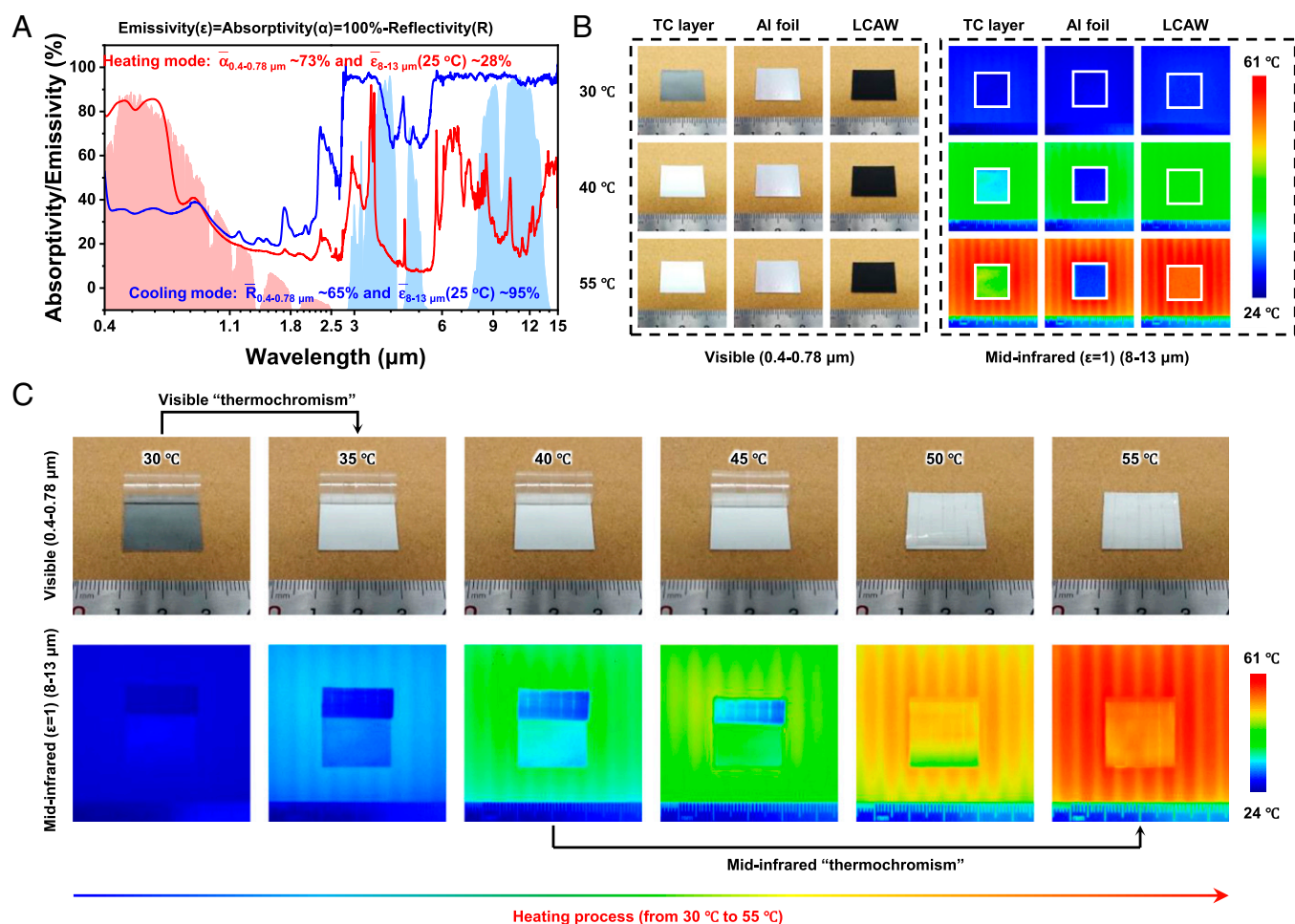


Fig. 3. Temperature-dependent spectral characteristics. (A) Spectral characteristics of the dual-mode device in heating and cooling modes along with normalized ASTM G173 Global solar spectrum (light-red area) and transparent infrared atmospheric window (US standard 1976, light-blue area). (B) Simultaneously captured optical and infrared images (set emissivity of 1) of TC layer, Al foil, and LCAW at different temperatures. The boundary of the sample is marked out by a white box in infrared images. (C) Simultaneously captured optical and infrared images (set emissivity of 1) of dual-mode device during the heating process of the heating plate, which visually present the visible and infrared thermochromism.

device. Then transparent tape-2W SMP film gradually unfolded and covered the white TC layer with the further increase of temperature, due to its temperature-sensitive shape change. The introduction of transparent tape-2W SMP film had little effect on the absorption of visible sunlight. In contrast, there was an obvious improvement in infrared emission (*SI Appendix, Fig. S7*). In the infrared images, the area in the dual-mode device covered by transparent tape-2W SMP film showed a high measured temperature close to that of the heating plate, while the uncovered area was a lower measured temperature. The dual-mode device in the intermediate state (50 °C) clearly presented this interesting infrared thermochromic phenomenon due to the huge difference of infrared emission between the covered and uncovered area. When the TC layer was completely covered by transparent tape-2W SMP film at 55 °C, the measured temperature of the whole dual-mode device was very close to that of the heating plate. A dynamic visible and infrared thermochromism of dual-mode device was displayed completely with its continuous morphology evolution during the whole heating process (*Movie S4*). Furthermore, we demonstrated that visible and infrared thermochromism of the dual-mode device could also be triggered by the ambient temperature, which is closer to reality (*SI Appendix, Fig. S8* and *Movie S5*).

Thermal Management Performance of the Dual-Mode Device.

Visible and infrared thermochromism of the dual-mode device had a great impact on its thermal management performance. We measured the enhancement of infrared emission with the unfolding of transparent tape-2W SMP film in the dual-mode device in the indoor environment. The device was attached to a heating plate and sealed in a foam chamber by a 10- μm -thick transparent polyethylene film (*SI Appendix, Figs. S9 and S10*). The room temperature was approximately 26 °C, and the calibrated parasitic heat-transfer coefficient (h_c) was 18.2 W/(m²·K) (*SI Appendix, Fig. S11*). A Joule heating power was applied to the device. According to the thermal balance relationship, the temperature of the dual-mode device in heating (red line) and cooling (blue line) modes with different Joule heating power was predicted in theory, respectively (*Fig. 4A*). The temperature of the device in cooling mode was always lower than that of the device in heating mode, which indicates the stronger ability of the device in cooling mode to transfer heat by infrared radiation. The measurements of the dual-mode device were consistent with predictions of the heating mode when the device was in heating mode under lower Joule heating power. As Joule heating power continues to increase, the measured temperatures gradually trended to predicted results of the cooling mode, accompanied by the spontaneous switch of the device from heating mode to cooling mode. It was noted that the measurements were slightly higher than predictions. This is related to the insufficient thermal contact between the transparent tape-2W SMP film and thermochromic substrate, when the device was in cooling mode. We also measured the indoor infrared radiative power (negative heat flux) of the dual-mode device at different temperatures (*Fig. 4B*). The predicted infrared radiative power of thermochromic substrate increased with increasing temperature according to Planck's law. Similarly, the measured infrared radiative power of the dual-mode device in heating mode agreed with the predicted value. Once the temperature was above the transition temperature of programmed 2W SMP, the radiative cooling power in measurements increased abruptly with the morphological evolution of temperature-sensitive actuator from coiled state to unfolding state. This extra infrared radiative power was exactly from the enhancement of infrared emissivity, corresponding to the device

switching from heating mode to cooling mode. As the temperature decreased, the infrared radiative power returned to a lower state, with the device automatically and reversibly switching back to the heating mode (*SI Appendix, Fig. S13*).

An outdoor field experiment in the real scenario was performed to test the practical thermal-management performance of the dual-mode device in a real environment (located on the campus of Nankai University in Tianjin [38.99N, 117.34E], People's Republic of China). To measure real-time solar heating power or radiative cooling power, two same-heat flux measurement systems were set up in parallel (*SI Appendix, Fig. S14*). Among them, one copper plate was covered by the dual-mode device, and the other was covered by a same-sized Al foil as a control, due to its near-perfect reflection for sunlight and infrared radiation (*SI Appendix, Fig. S5*). A feed-back controlled Joule heating power maintained the measured temperature of the device the same as that of Al foil to minimize the impacts of conductive and convective heat losses (*SI Appendix, Fig. S15*). In this state, the difference in Joule heating power of Al foil minus that of the dual-mode device was defined as solar heating power (positive heat flux) or radiative cooling power (negative heat flux). Under the direct solar radiation in a clear sky, a 2 h continuous measurement showed that the device in heating and cooling modes could achieve an average solar heating power of ~ 252.2 W/m² and an average radiative cooling power of ~ 59.7 W/m², respectively (*Fig. 4C*). However, the measured results of the field experiment showed that the dual-mode device realized the switch of thermal-management mode between heating and cooling based on visible and infrared thermochromism, rather than a simple modulation of heating or cooling power.

According to the typical meteorological data, we quantitatively estimated the potential of our dual-mode device on all-season energy saving (*SI Appendix, Note S4*). Tianjin, with a temperate monsoon climate, was chosen as an example. As expected, the maximum energy saving for heating happened at solar absorptivity (α_{solar}) of 100% and infrared emissivity ($\epsilon_{\text{infrared}}$) of 0% (*Fig. 4D*). In contrast, the maximum energy saving for cooling occurred at solar reflectivity of 100% (0% α_{solar}) and 100% $\epsilon_{\text{infrared}}$ (*Fig. 4E*). The closer the spectral characteristic of the thermal-management device was to the ideal electromagnetic spectrum, the better was the energy-saving effect. Two-way temperature control was the most distinct characteristic of our dual-mode device, rather than only modulating heating or cooling power, like most reported one-way temperature-responsive devices. Benefiting from two opposite highly selective electromagnetic spectrums, the dual-mode device could provide all-season energy saving for temperature control—heating up in cold winter and cooling down in hot summer—instead of undesired radiative cooling in cold winter or solar heating in hot summer. We made a calculation for all-season energy saving of our device and other representative temperature-responsive thermal-management devices reported in the literature (*Fig. 4F*). The predicted results show that our device had the greatest potential for energy saving in terms of temperature control among them. In addition, there was a certain gap of electromagnetic spectrum between our dual-mode device, which carries a considerable potential for energy saving in thermal management, and ideal materials.

Discussion

In summary, we demonstrated a dynamic thermal-management device based on visible and infrared thermochromism without any external energy consumption. Inspired by the color change

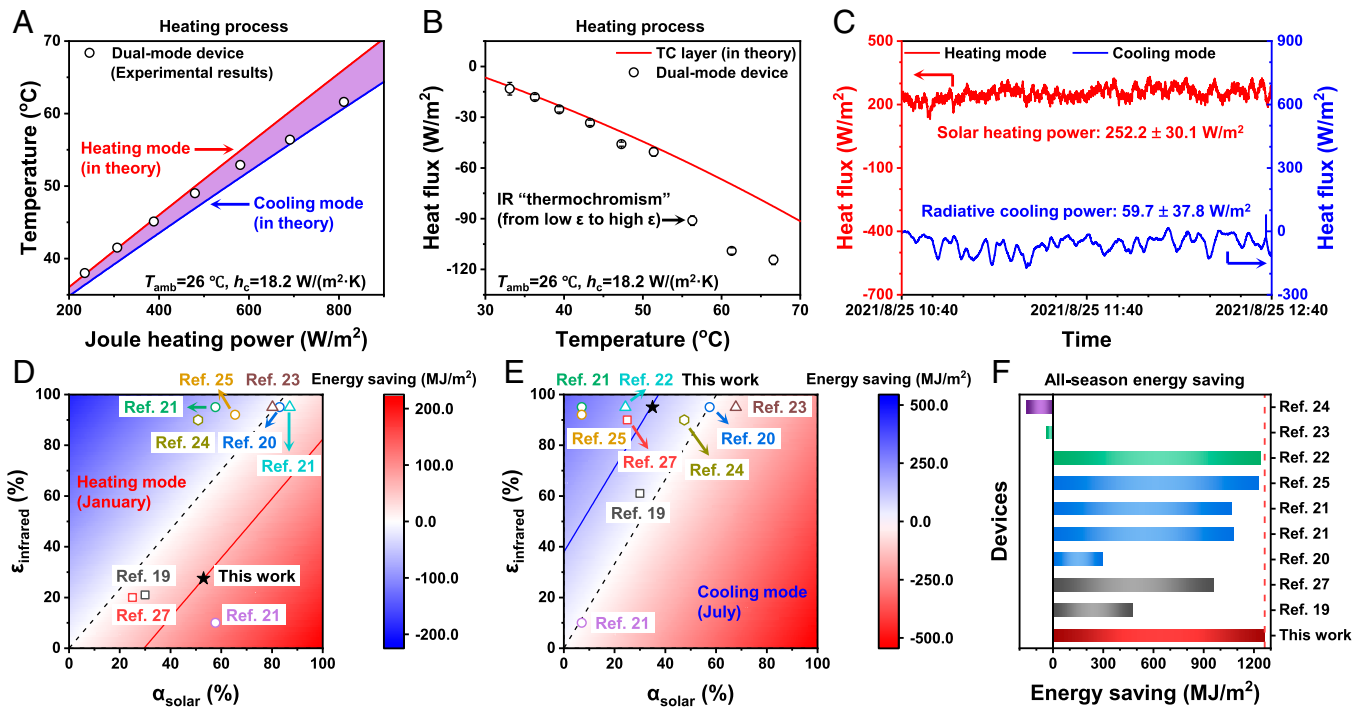


Fig. 4. Thermal-management performance of the dual-mode device. (A) Temperature of the dual-mode device (black circle) applied with different Joule heating power during the heating process, compared with prediction of a dual-mode device in heating (red line) or cooling mode (blue line) in theory. (B) Measured cooling power of a dual-mode device (black circle) and predicted cooling power of an individual thermochromic substrate (red line) as a function of heating temperature during the heating process. The indoor temperature was $\sim 26^\circ\text{C}$. (C) Continuous time-resolved solar heating power (red) and radiative cooling power (blue) measured in an open-space outdoor environment. (D and E) Mapping results on the effects of solar absorptivity and infrared (IR) emissivity to the energy saving for (D) heating in January and (E) cooling in July in Tianjin. Solar absorptivity and infrared emissivity of the dual-mode device (black star) is compared with those of temperature-responsive thermal-management devices in the literature. These thermal-management devices are divided into four categories according to the major components: modified vanadium dioxide (VO_2) (square), hydrogel (circle), phase-changing polymer (triangle), and other materials (hexagon). Dashed line is a line of demarcation between energy saving and energy consumption. Red and blue lines are the iso-potential lines of energy saving of the dual-mode device in heating mode in January and cooling mode in July, respectively. (F) All-season potential energy saving of the dual-mode device (red bar and dashed line) in Tianjin compared with other temperature-responsive thermal-management devices reported in the literature. Modified VO_2 (black), hydrogel (blue), phase-changing polymer (green), and other materials (purple).

of the Himalayan rabbit's hair and folding-opening movement of *M. pudica*'s leaves, simultaneous modulation of spectral characteristics in two separate wavelength ranges was realized. This unique ability enables the device to switch between heating mode ($\alpha_{0.4-0.78\ \mu\text{m}}$ of 73% and $\varepsilon_{8-13\ \mu\text{m}}$ of 28%) and cooling mode ($R_{0.4-0.78\ \mu\text{m}}$ of 65% and $\varepsilon_{8-13\ \mu\text{m}}$ of 95%), rather than simply adjusting heating power or cooling power. The trigger temperature of the device is also adjustable to meet the demands in different application fields. Numerical prediction shows our device has the best effect of all-season energy saving for temperature control compared with the temperature-responsive thermal-management devices in the literature. This thermal-management strategy based on multiple thermochromism provides a platform to realize the full potential of solar heating and radiative cooling in terms of energy saving.

By using renewable energy in nature, solar heat, and space cold, the thermal-management device could realize a dynamic temperature control without any external energy consumption. Referring to the reported studies, this device is well suited for initial temperature control of heat-transfer fluid in active thermal-management systems. It will significantly improve thermal energy utilization efficiency, although there is still a lot of room for improvement in solar heating power and radiative cooling power. On the other hand, the strategy to trade morphology for electromagnetic property provides an instructive route to independently modulate spectral characteristics of different wavebands in an integrated system. After precise optimization of the triggering condition and target waveband, this strategy is expected to be

applied to the broader field of dynamic modulation of electromagnetic properties in the future.

Materials and Methods

Raw Materials. PTHF ($M_w = 2,900$), PCL ($M_w = 10,000/36,000$), PCL-diol ($M_w = 2,000$), HDI (99%), DBTDL (95%), ethyl alcohol (99.7%), and *N,N*-dimethylformamide (DMF, 99.9%) were purchased from Shanghai Aladdin Biochemical Technology Co., Ltd. Rutile titanium dioxide nanoparticles (TiO_2 NPs) were purchased from Shanghai Yaoyi Co. Ltd. Trichloromethane (CHCl_3 , AR) was purchased from Tianjin Bohua Chemical Reagents Co., Ltd. All materials were used without any further purification.

Preparation of Thermochromic Substrate. Thermochromic substrate was prepared by blade-coating technology. We fully dissolved 1 g of NBR in 50 mL of DMF by stirring at 80°C . Meanwhile, 0.27 g of thermochromic powder and 0.03 g of TiO_2 NPs were dispersed in 3 mL of ethyl alcohol by tip ultrasonication (200 W, 30 min) to make a precursor of thermochromic layer. The NBR solution was blade-coated onto a flat Al foil to fabricate the uniform liquid film between two spacers of $40\text{-}\mu\text{m}$ -thick transparent tape, which was placed on an 80°C heating plate immediately to rapidly evaporate solvent. Then, the precursor of the thermochromic layer was blade-coated on NBR-coated Al foil, which was also placed on the 80°C heating plate. After evaporation of solvent, thermochromic powders and TiO_2 NPs were fixed on the Al foil by NBR to form a thermochromic substrate.

Synthesis of 2W SMP. 2W SMP was synthesized by one-step esterification reactions between three monomers on the catalyst. PTHF and PCL (or PCL-diol) were fully dissolved in CHCl_3 by stirring at room temperature. Then, HDI and DBTDL were added into the solution in sequence, which was stirred constantly

for 3.5 h at room temperature. The molar ratio of the three monomers ($n_{\text{PTHF}}:n_{\text{PCL}}:n_{\text{HDI}}$) was 9:1:20. The amount of DBTDL catalyst was 1% of the total weight of the three monomers. With the help of the catalyst, the monomers could polymerize gradually into prepolymer of 2W SMP. The product was poured into a horizontal stainless-steel Petri dish. After complete volatilization of the solvent at room temperature, a 2W SMP film existed at the bottom of the Petri dish, which could be cut into any shape as required.

Characterization. The reflective spectra of the dual-mode device in heating and cooling modes were measured by using an ultraviolet-visible near-infrared spectrophotometer (Cary 5000, Agilent) with a calibrated integrating sphere and a Fourier transform infrared spectrometer (Frontier Optica, Perkin Elmer) with an integrating sphere (MCT Mid-IR Integrated Sphere, Pike). The absorptivity/emissivity (α/ϵ) was calculated using 100% reflectivity (0% transmissivity determined by Al foil). Temperature-dependent XRD data were measured by X-ray powder diffraction

instrument (Smart Lab SE, Rigaku) with a homemade proportional-integral-derivative (PID) temperature control setup. Optical and infrared images were captured by an optical camera (FDR-AXP55, Sony) and an infrared camera, respectively.

Data, Materials, and Software Availability. All study data are included in the article and/or supporting information.

ACKNOWLEDGMENTS. This work is supported by the National Key R&D Program of China (2020YFA0711500 and 2020YFA0711501) and the National Natural Science Foundation of China (51973095 and 52011540401).

Author affiliations: ^aSchool of Materials Science and Engineering, National Institute for Advanced Materials, Nankai University, Tianjin, 300350 People's Republic of China

1. J. Wang *et al.*, Recent active thermal management technologies for the development of energy-optimized aerospace vehicles in China. *Chin. J. Aeronaut.* **34**, 1–27 (2021).
2. N. Egidij, P. Maponi, L. Misici, S. Rubino, A three-dimensional model for the study of the cooling system of submersible electric pumps. *Math. Comput. Simul.* **82**, 2962–2970 (2012).
3. J. Shi *et al.*, Electrocaloric cooling materials and devices for zero-global-warming-potential, high-efficiency refrigeration. *Joule* **3**, 1200–1225 (2019).
4. J. Tusek *et al.*, A regenerative elastocaloric heat pump. *Nat. Energy* **1**, 16134 (2016).
5. R. Wang *et al.*, Torsional refrigeration by twisted, coiled, and supercoiled fibers. *Science* **366**, 216–221 (2019).
6. F. Greibich *et al.*, Elastocaloric heat pump with specific cooling power of 20.9 W g⁻¹ exploiting snap-through instability and strain-induced crystallization. *Nat. Energy* **6**, 260–267 (2021).
7. S. Hong *et al.*, Wearable thermoelectrics for personalized thermoregulation. *Sci. Adv.* **5**, eaaw0536 (2019).
8. International Energy Agency, World energy outlook 2020. <https://www.iea.org/reports/world-energy-outlook-2020>. Accessed 29 September 2021.
9. International Energy Agency, Renewable energy policies in a time of transition: Heating and cooling. <https://www.iea.org/reports/renewable-energy-policies-in-a-time-of-transition-heating-and-cooling>. Accessed 15 March 2021.
10. G. L. Stephens, T. L'Ecuyer, The Earth's energy balance. *Atmos. Res.* **166**, 195–203 (2015).
11. X. Yin, R. Yang, G. Tan, S. Fan, Terrestrial radiative cooling: Using the cold universe as a renewable and sustainable energy source. *Science* **370**, 786–791 (2020).
12. L. Zhou *et al.*, Hybrid concentrated radiative cooling and solar heating in a single system. *Cell Rep. Phys. Sci.* **2**, 100338 (2021).
13. X. Li *et al.*, Integration of daytime radiative cooling and solar heating for year-round energy saving in buildings. *Nat. Commun.* **11**, 6101 (2020).
14. H. Luo *et al.*, Outdoor personal thermal management with simultaneous electricity generation. *Nano Lett.* **21**, 3879–3886 (2021).
15. Y. Rao *et al.*, Ultra-wideband transparent conductive electrode for electrochromic synergistic solar and radiative heat management. *ACS Energy Lett.* **6**, 3906–3915 (2021).
16. J. Mandal *et al.*, Scalable, “dip-and-dry” fabrication of a wide-angle plasmonic selective absorber for high-efficiency solar-thermal energy conversion. *Adv. Mater.* **29**, 1702156 (2017).
17. D. Zhao *et al.*, Radiative sky cooling: Fundamental principles, materials, and applications. *Appl. Phys. Rev.* **6**, 021306 (2019).
18. A. T. D. Perera, V. M. Nik, D. Chen, J.-L. Scartezini, T. Hong, Quantifying the impacts of climate change and extreme climate events on energy systems. *Nat. Energy* **5**, 150–159 (2020).
19. S. Wang *et al.*, Scalable thermochromic smart windows with passive radiative cooling regulation. *Science* **374**, 1501–1504 (2021).
20. Y. Zhou, Y. Cai, X. Hu, Y. Long, Temperature-responsive hydrogel with ultra-large solar modulation and high luminous transmission for “smart window” applications. *J. Mater. Chem. A* **2**, 13550–13555 (2014).
21. S. Wang *et al.*, Thermochromic smart windows with highly regulated radiative cooling and solar transmission. *Nano Energy* **89**, 106440 (2021).
22. Y. Liu *et al.*, Automatically modulated thermoresponsive film based on a phase-changing copolymer. *Chem. Mater.* **33**, 7232–7241 (2021).
23. Q. Zhang *et al.*, Ultra-compliant and tough thermochromic polymer for self-regulated smart windows. *Adv. Funct. Mater.* **31**, 2100686 (2021).
24. S. Liu *et al.*, Self-densified optically transparent VO₂ thermochromic wood film for smart windows. *ACS Appl. Mater. Interfaces* **13**, 22495–22504 (2021).
25. C. Lin *et al.*, All-weather thermochromic windows for synchronous solar and thermal radiation regulation. *Sci. Adv.* **8**, eabn7359 (2022).
26. Y. Wang, J. Ren, C. Ye, Y. Pei, S. Ling, Thermochromic silks for temperature management and dynamic textile displays. *Nano-Micro Lett.* **13**, 72 (2021).
27. K. Tang *et al.*, Temperature-adaptive radiative coating for all-season household thermal regulation. *Science* **374**, 1504–1509 (2021).
28. X. Wu *et al.*, Passive smart thermal control coatings incorporating CaF₂/VO₂ core-shell microsphere structures. *Nano Lett.* **21**, 3908–3914 (2021).
29. M. Ono, K. Chen, W. Li, S. Fan, Self-adaptive radiative cooling based on phase change materials. *Opt. Express* **26**, A777–A787 (2018).
30. J. Gu *et al.*, VO₂-based infrared radiation regulator with excellent dynamic thermal management performance. *ACS Appl. Mater. Interfaces* **14**, 2683–2690 (2022).
31. X. Ao *et al.*, Self-adaptive integration of photothermal and radiative cooling for continuous energy harvesting from the sun and outer space. *Proc. Natl. Acad. Sci. U.S.A.* **119**, e2120557119 (2022).
32. X. Li *et al.*, Metalized polyamide heterostructure as a moisture-responsive actuator for multimodal adaptive personal heat management. *Sci. Adv.* **7**, eabj7906 (2021).
33. X. A. Zhang *et al.*, Dynamic gating of infrared radiation in a textile. *Science* **363**, 619–623 (2019).
34. R. Liu *et al.*, High-efficiency solar heat storage enabled by adaptive radiation management. *Cell Rep. Phys. Sci.* **2**, 100533 (2021).
35. E. M. Leung *et al.*, A dynamic thermoregulatory material inspired by squid skin. *Nat. Commun.* **10**, 1947 (2019).
36. H. Fang *et al.*, A triple-mode midinfrared modulator for radiative heat management of objects with various emissivity. *Nano Lett.* **21**, 4106–4114 (2021).
37. S. Zeng *et al.*, Dynamic thermal radiation modulators via mechanically tunable surface emissivity. *Mater. Today* **45**, 44–53 (2021).
38. H. Zhang *et al.*, Biologically inspired flexible photonic films for efficient passive radiative cooling. *Proc. Natl. Acad. Sci. U.S.A.* **117**, 14657–14666 (2020).
39. S. Dou *et al.*, Bioinspired microstructured materials for optical and thermal regulation. *Adv. Mater.* **33**, 2000697 (2021).
40. J. Yang *et al.*, Beyond the visible: Bioinspired infrared adaptive materials. *Adv. Mater.* **33**, 2004754 (2021).
41. L. Wang, A. M. Urbas, Q. Li, Nature-inspired emerging chiral liquid crystal nanostructures: From molecular self-assembly to DNA mesophase and nanocolloids. *Adv. Mater.* **32**, 1801335 (2020).
42. J. Hoddinott, Rates of translocation and photosynthesis in *Mimosa pudica* L. *New Phytol.* **79**, 269–272 (1977).
43. I. Bellin, S. Kelch, R. Langer, A. Lendlein, Polymeric triple-shape materials. *Proc. Natl. Acad. Sci. U.S.A.* **103**, 18043–18047 (2006).
44. L. Du *et al.*, From a body temperature-triggered reversible shape-memory material to high-sensitive bionic soft actuators. *Appl. Mater. Today* **18**, 100463 (2020).
45. M. Behl, K. Kratz, J. Zotzmann, U. Nöckel, A. Lendlein, Reversible bidirectional shape-memory polymers. *Adv. Mater.* **25**, 4466–4469 (2013).